Computation of electrodynamic forces acting on clamping beams of windings in power transformers

Cuong Nguyen Vu[1], Thanh Nguyen Vu[2], Hung Bui Duc[2], Dung Dang Chi[2], Bao Doan Thanh[3] and Vuong Dang Quoc[2]

[1]Dong Anh Electrical Equipment Corporation - Joint Stock Company
[2]School of Electrical and Electronic Engineering, Hanoi University of Science and Technology
[3]Quy Nhon University
[*]Corresponding author E-mail: vuong.dangquoc@hust.edu.vn
DOI: https://doi.org/10.64032/mca.v29i3.347

Abstract

In response to the growing demand for electrical load driven by socio-economic development, the national transmission grid is being gradually upgraded. In this context, conventional power transformers with capacities of 3x150 MVA-500kV and 3x200 MVA-500kV are increasingly being replaced by higher-capacity units, most notably the 3×300 MVA transformers. To meet this trend and reduce dependence on imported equipment, the research, design, and manufacturing of power transformer with 3x300 MVA-500kV present a significant technological challenge for the domestic industry and remain a current topic of interest among both national and international researchers. During operation, short-circuit events subject the windings to extremely high electrodynamic forces, posing a risk of severe deformation or insulation failure if not properly designed. In the winding structures, the clamping beam plays a critical role in directly withstanding these forces, preserving the mechanical integrity of the winding, and maintaining insulation stability throughout operation. This paper develops an analytical approach combined with the finite element method (FEM) to compute, analyze and simulate the electrodynamic forces and deformation acting on the clamping beam in supper-high voltage transformers with power ratings up to 300 MVA-500kV under various operating conditions. Accurate assessment of the mechanical behavior during short-circuit events is essential to ensure the structural integrity and safe operation of the equipment.

***Keywords**: Super high voltage transformer; clamping beam; electrodynamic force, mechanical stress; FEM.*

Symbols

Symbols	Units	Description
A(x,y,z)	A	Magnetic vector potential
B	Testa	Magnetic flux density
H		d and q stator inductance
μ	H/m	Relative permeability
J	A/m^2	Electric current density
i_{hos}	Ampere	is the harmonic oscillation;
i_{dos}	Ampere	is the damped oscillation;
ω	(rad/s);	is the angular frequency
ϕ	rad	Angle at the moment of SC
t	s	time
I_{cs}	A	Short circuit current
F_{total}	N	Total forces
D_m	Mm	Medium clamping beam diameter
c	mm	Radial clamping beam width
h	mm	Thickness of clamping beam
n	Points	Number of clamping (pressing) points
M_1	N.m	Corresponding bending moment
W	Number	Section modulus of the clamping beam
σ_{1max}, σ_{2max}	$\frac{kgf}{cm^2}$	maximum bending stress

1. Introduction

Power transformers represent some of the most capital-intensive components within electric power transmission and distribution networks. Their safe and reliable operation is essential to system stability, making monitoring and mechanical integrity of key importance. Modern transformer monitoring systems focus primarily on thermal performance, bushing condition, and main insulation health, transmitting real-time diagnostic data to control centers. While such systems can identify thermal or insulation-related issues, they often overlook a critical aspect of transformer longevity: the mechanical stability of the winding axial clamping beam system. The clamping beam system must ensure consistent compression of the windings throughout the transformer's service life, despite the influence of electrodynamic forces, temperature fluctuations, and material aging. Most power transformers utilize rigid clamping mechanisms that apply an initial compression based on expected short-circuit forces, the mechanical properties of insulation, and manufacturing constraints. In certain applications, especially those with higher operational demands, specialized axial clamping structures are employed.

Up to the present time, numerous studies have been conducted on the electromagnetic forces acting on transformer windings, specifically including: In [1-2], a combined approach using MATLAB and the finite element method (FEM) was employed to calculate the magnetic field, short-circuit current, and resulting electromagnetic forces in a 3-phase amorphous transformer (22/0.4 kV) under short-circuit fault conditions. In [3] presented an analysis in which the maximum short-circuit current and the short-circuit voltage across the phases of the low-voltage (LV) winding were determined. Based on these parameters, the maximum axial and radial distributions of electromagnetic forces acting on both the high-voltage (HV) and LV windings were evaluated. The findings indicate that the interaction between the maximum short-circuit current-whether in one, two, or all three phases-and the magnetic field within the windings

Received: 07 June 2025; Revised: 02 July 2025; Accepted: 04 July 2025.

generates significant electromagnetic forces. In [4, 5], authors investigated and analyzed the axial and radial electromagnetic forces (EMFs) acting on the LV and HV windings of an amorphous core transformer using two distinct approaches: an analytical method and a 3D FEM. In [6, 7], the paper presented a foundation for comprehensive studies on the mechanical stability of power transformers through continuous operational monitoring. According to [8], the study demonstrated that under single phase-to-ground short-circuit conditions, the leakage flux density in transformer windings increases markedly. This elevated flux density, combined with higher current density, results in a significant increase in the electromagnetic forces exerted on the windings. In [9], a 3D model of a large transformer, based on a real-world unit, is developed for simulation purposes. The simulation results indicated that, following a short-circuit event, the leakage flux is predominantly concentrated in the gap between the HV and LV windings. In [10], the paper investigated short-circuit electromagnetic forces in transformers, which have increased due to the rise of supper-high voltage systems. Using both analytical methods and 2D/3D finite element simulations, the study accurately calculates these forces and validates results against measured data. The findings offer a reliable basis for improving transformer design and ensuring structural integrity under fault conditions.

This paper proposes a combined analytical approach and FEM to calculate and simulate the electrodynamic forces and stress acting on clamping beams of power transformer windings rated up to 300MVA-500kV under various fault scenarios. The accurate assessment of mechanical response under short-circuit stress is essential to ensure structural reliability and operational safety. The FEM developed enables the detailed evaluation of stress and deformation behavior across different support regions, contributing to improved transformer design methodologies.

2. Analytical background

Based on the the Laplace-Poisson's equation, in three dimension, the magnetic vector potential **A**(x,y,z) is written via the Maxwell's equations [1]-[3]:

$$\frac{\partial^2 \mathbf{A}(x,y,z)}{\partial x^2}+\frac{\partial^2 \mathbf{A}(x,y,z)}{\partial y^2}+\frac{\partial^2 \mathbf{A}(x,y,z)}{\partial z^2}=-\mu\,\mathbf{J} \qquad (1)$$

where:

$$\nabla^2 \mathbf{A}(x,y,z)=\begin{cases}-\mu\mathbf{J} & \text{in the windings}\\ 0 & \text{others}\end{cases} \qquad (2)$$

The magnetic flux density (**B**) can be defined via the term **A,** that is,

$$\mathbf{B}=\text{curl}\ \mathbf{A} \qquad (3)$$

The boundary conditions of **B** in the x- and y- axis can be expressed as [1]-[3]:

$$\begin{cases}B_x=\dfrac{\partial \mathbf{A}(x,y)}{\partial y}\\ B_y=-\dfrac{\partial \mathbf{A}(x,y)}{\partial x}\end{cases} \qquad (4)$$

In the case of the short-circuit transformer is considered. The short-circuit current in the windings can potentially damage the transformer. This transient current consists of two distinct components [1]-[4]:

$$i_{short\ circuit\ (SC)}=i_{dos}+i_{hos}=\frac{U_{nominal}}{Z_{Sc}}\sqrt{2}\sin(\omega t-\phi-\varphi_{sc})+\frac{U_{nominal}}{Z_{Sc}}\sqrt{2}\sin(\phi+\varphi_{sc})\,e^{-\frac{R_{SC}}{X_{SC}}\omega t} \qquad (5)$$

where $U_{Nominal}$ is nominal voltage, R_{SC} is the resistance, X_{SC} is the reactance and Z_{SC} is the SC impedance (Ω).

3. Electrodynamic Forces and Mechanical stressing Acting on Clamping Beams

The structural response of transformer windings to axial forces encountered during operation is governed by a combination of factors, including winding geometry, insulation system configuration, and the effectiveness of the axial clamping mechanism. Adequate axial compression is essential for maintaining winding alignment and mechanical integrity under dynamic electrical loading conditions. However, current pressing systems used in transformer manufacturing often exhibit limitations in uniformly distributing compression forces across windings located on the same magnetic core column. These limitations primarily stem from inherent design constraints, material variations, and manufacturing tolerances. The clamping beam systems are generally for an assembly of windings as shown in Figure 1 [5].

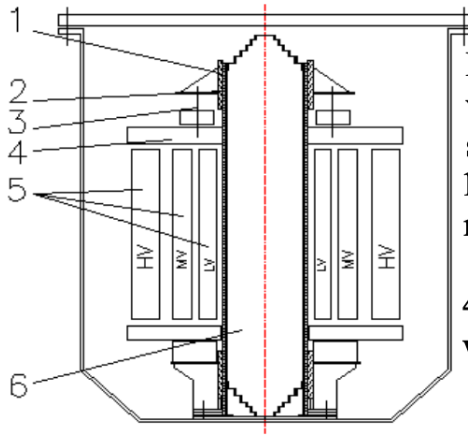

Figure 1: Modeling of winding clamping beam: 1-frame works; 2-tie rod plages; pressing plate; 4-clamping beam; 5-LV, HV and MV windings; 6-iron core of transformer [5].

Although the low, medium, and high-voltage windings within a single transformer limb have identical geometric heights, they differ significantly in construction due to variations in active material content (copper and insulation), determined by their specific electrical characteristics (voltage, current, coil type, etc.). Consequently, the degree of compressibility varies, leading to unequal axial clamping forces when a common clamping system is applied. To address this issue, independent clamping systems for each winding are recommended. Considering the impact of axial compression on long-term transformer performance, it is advisable to implement advanced axial force monitoring systems, such as the one developed by ICMET [6], [7], where construction and technology permit.

Common clamping rings are the primary components susceptible to damage from electrodynamic forces during short-circuit events. These forces cause deformation in the ring segments located between adjacent clamping bolts. Therefore, accurately determining the forces acting on transformer board rings is essential to identify the critical stress levels leading to failure. As a first approximation, the stress on a clamping ring can be evaluated by assuming that the forces are applied at the bolt locations [5]. The maximum bending stress is given as [5]:

$$\sigma_{1max} = \frac{M_1}{W}, \quad (6)$$

where M_1 is the corresponding bending moment and W is the section modulus of the clamping beam. The terms of M_1 and W can then be calculated accordingly [5], [11]-[15]:

$$M_1 = \frac{F_{at}\pi D_m}{8n^2}\ [\text{kgf. cm}], \qquad W = \frac{1}{6}ch^2 \quad (7)$$

By substituting (7) into (6), one gets:

$$\sigma_{1max} = \frac{M_1}{W} = \frac{3\pi F_{total} D_m}{4ch^2n^2}\ \left[\frac{kgf}{cm^2}\right], \quad (8)$$

When the clamping beam is combined with the fixed beam, the resulting bending moment (M_2) is given by [5]:

$$M_2 = \frac{F_{total}\pi D_m}{12n^2}\ \left[\frac{\text{kgf}}{\text{cm}^2}\right] \quad (9)$$

From the equation (9), the maximum bending stress is defined by relation:

$$\sigma_{2max} = \frac{M_2}{W} = \frac{6\pi F_{at} D_m}{12ch^2n^2} = \frac{\pi F_{at} D_m}{2ch^2n^2}\ \left[\frac{kgf}{cm^2}\right] \quad (10)$$

By comparing relations (3) and (5), one has:

$$\sigma_{1max} > \sigma_{2max} \quad (11)$$

In the design process, the stress can be estimated using the average of the two moments defined above [5].

$$M_3 = \frac{\pi F_{at} D_m}{10n^2}\ \left[\frac{kgf}{cm^2}\right] \quad (12)$$

Finally, the bending stress is given as [5]:

$$\sigma_{3max} = \frac{M_3}{W} = \frac{6\pi F_{at} D_m}{10ch^2n^2} = \frac{3\pi F_{at} D_m}{5ch^2n^2}\ \left[\frac{kgf}{cm^2}\right] \quad (13)$$

The calculated value must remain within the allowable limits defined by the material properties and the applied safety factor.

4. Finite element results and discussion

In this part, the practical test is the clamping beam of high voltage transformer (300MVA-500kV) as shown in Figure 2. The main body of the clamping beam is made of high-strength steel AH36 with a yield stress of σ_y = 355 MPa. The column cover is made of structural stainless steel SUS304 with a yield stress of σ_y = 240 MPa. The tensioning components use fiberglass straps with a tensile strength of 3000 MPa. The test problem is considered with diferent cases:

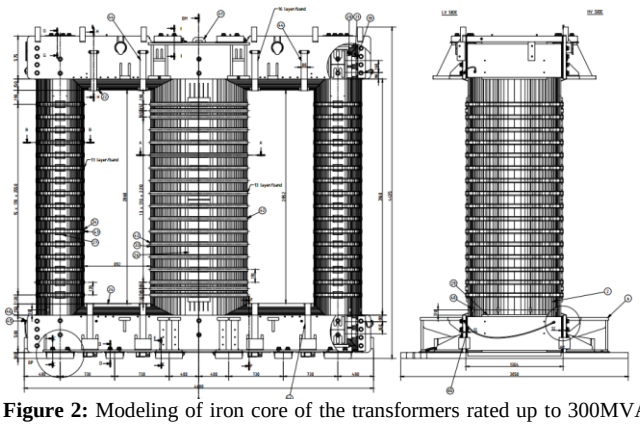

Figure 2: Modeling of iron core of the transformers rated up to 300MVA-500kV

4.1 FEM analysis of upper clamping beam deformation caused by winding clamping during installation:

The model of the upper clamping beam during installation is pointed out in Figure 3. It can be seen that the total clamping force required for winding compression during assembly must be carefully calculated to ensure structural stability and avoid premature deformation: $F_{total} = 1764\ kN$. The total contact area of the four pressing surfaces is calculated as $S_1 = 0.164.10^6$ mm², serving as the basis for determining the required axial clamping force during winding assembly.

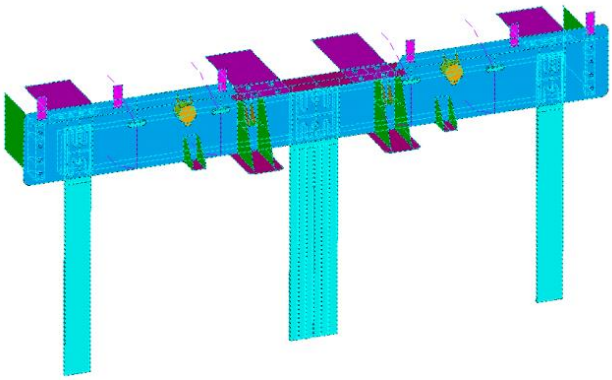

Figure 3: Model of the upper clamping beam during installation.

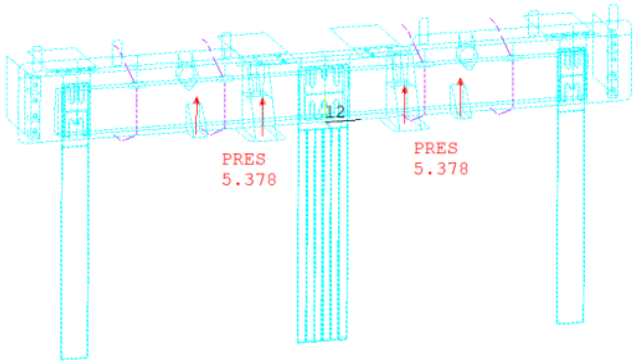

Figure 4: Distribution of component forces on the clamping beam during the winding compression process.

Thus, the pressure applied at a single clamping point is calculated as:

$$P_1 = \frac{F_{total}}{S_1} = \frac{1764000}{2x0{,}164x10^6} = 5.378\frac{N}{mm^2} \qquad (14)$$

Figure 4 illustrates the distribution of component forces on the clamping beam during the winding compression process, highlighting areas of non-uniform stress transmission.

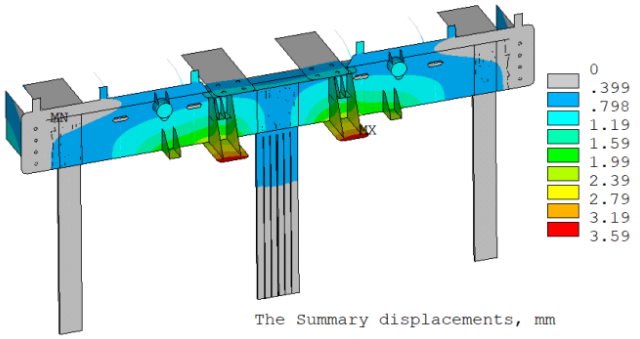

Figure 5: Simulation results of clamping beam deformation during winding compression

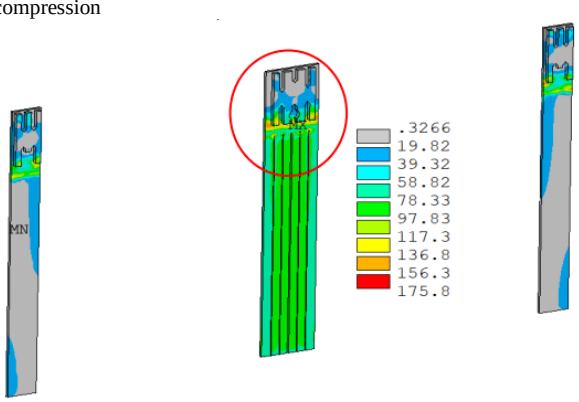

Figure 6: Stress concentrations at structural interfaces between core brackets and clamping beam.

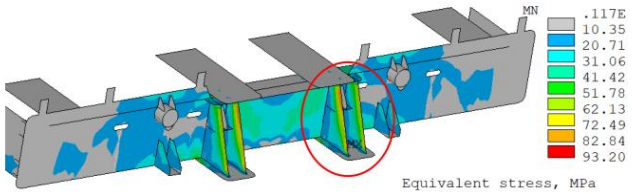

Figure 7: Simulated stress levels at the support wedges used in winding compression during assembly.

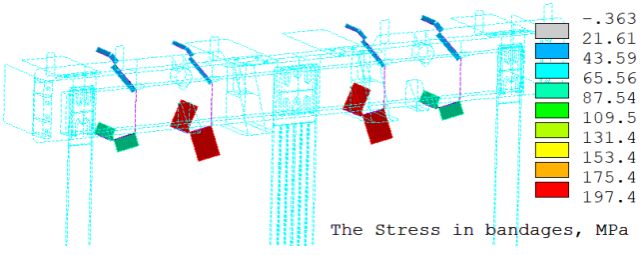

Figure 8: Response of simulated stress at core banding attachment points.

Figure 5 shows the simulation results of clamping beam deformation during winding compression, indicating areas of maximum axial displacement and stress concentration. The maximum value for this case is 3.59 N/mm. The simulation revealed elevated stress levels at the core clamping bracket locations connected to the clamping beam, indicating critical zones for mechanical reinforcement is shown in Figure 6. In the same way, the simulated stress levels at the support wedges used in winding compression during assembly is presented in Figure 7. It can be seen that the FEM simulation identified notable stress concentrations at the wedge block locations during winding compression, which are critical for maintaining axial stability. The FEM simulations further reveal notable stress concentrations at the magnetic core banding locations, which are critical for structural stability under dynamic conditions, is indicated in Figure 8.

4.2 Simulation of upper clamping beam deformation during magnetic core lifting in the assembly process:

The total weight of the magnetic core was calculated to be 93,020 kg, which contributes significantly to axial loading conditions on the clamping structure. The stressure exerted on the lifting lug positions is defined as:

$$P_2 = \frac{F_{total}}{4S_2} = \frac{93020x9{,}81}{4x21992} = 10.37\frac{N}{mm^2}, \qquad (15)$$

where S_2 represents the contact area at the lifting pin interface: $S_2 = 21992$ (mm^2).

In the similar way, the pressure exerted on the winding press-block locations:

$$P_3 = \frac{F_{total}}{4S_1} = \frac{0.7x\ 1764000}{4x0{,}164x10^6} = 3.3765\frac{N}{mm^2}, \qquad (16)$$

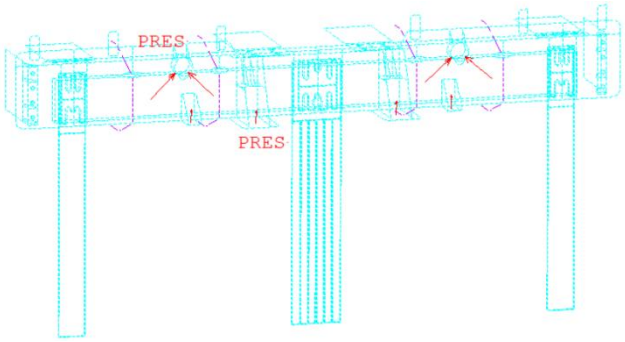

Figure 9: Force distribution mesh on the clamping beam during active part lifting.

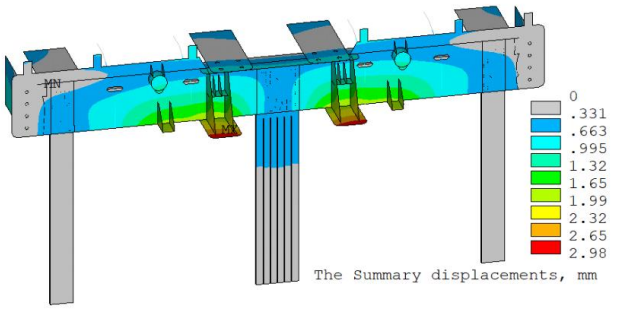

Figure 10: Simulation results of clamping beam deformation during active part lifting.

Figure 9 shows the force distribution mesh on the clamping beam during active part lifting, highlighting areas of concentrated loading around the lifting lugs. Figure 10 presents the simulation results of clamping beam deformation during active part lifting, revealing critical stress zones around the lifting lugs and guiding reinforcement design.

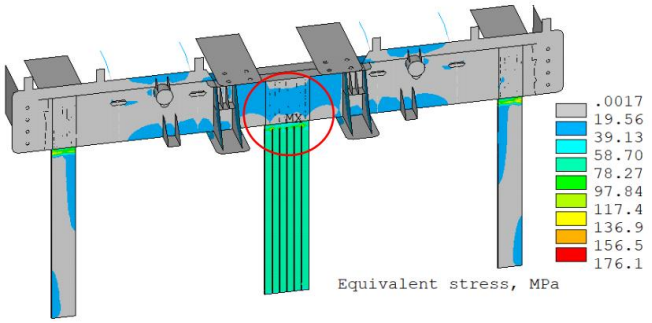

Figure 11: Simulated stress at the structural brackets connecting the core to the clamping beam.

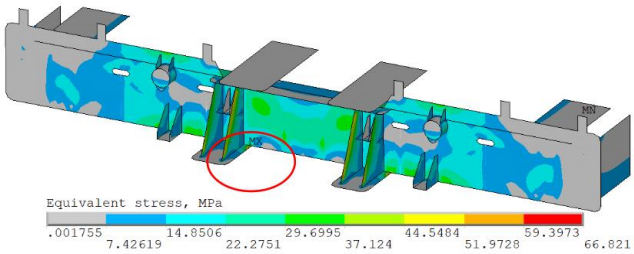

Figure 12: Stress results at the winding wedge locations during active part lifting.

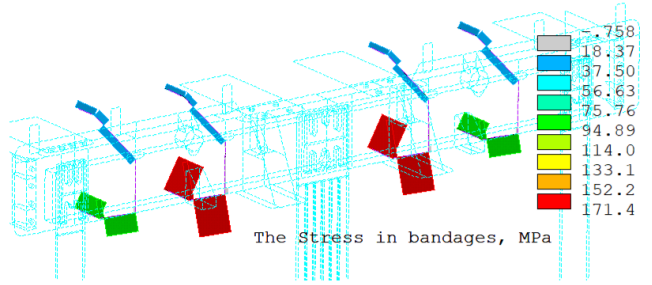

Figure 13: Stress results at the magnetic core banding locations during lifting.

In Figure 11, the FEM simulations revealed significant stress concentrations at the core bracket locations, indicating critical zones for structural reinforcement to maintain core alignment and stability. In Figure 12, the FEM results show increased stress at the winding wedge locations during the hoisting process, which may lead to localized deformation if not properly reinforced. The simulation revealed localized stress accumulation at the magnetic core banding locations during hoisting, indicating a need for mechanical reinforcement in these regions (Figure 13).

4.3 Simulation of upper clamping beam deformation during short-circuit conditions:

- The electrodynamic force exerted on the upper clamping beam by the LV winding during short-circuit conditions is: F_{LV}=246 kN.
- The electrodynamic force from the medium-voltage (MV) winding is: F_{MV}=1,584 kN.
- The HV winding contributes a force is: F_{HV}=1,584 kN.
- The regulating voltage (RV) winding applies a force is: F_{RV}=1,584 kN.
- The total short-circuit force transmitted to the upper clamping beam from all windings is therefore:

$$\sum F_{total} = F_{LV} + F_{MV} + F_{HV} + F_{RV} \quad (17)$$

=246 kN+1584 kN+1662 kN+219 kN = 3711 kN

- So, the pressure exerted on the yoke wall during a short circuit.

$$P_4 = \frac{\sum F_{total}}{4S_1} = \frac{3711000}{2x0{,}164x10^6} = 11.3\frac{N}{mm^2}, \quad (18)$$

where S_1 is the area of the four contact surfaces (S_1 = 0.164. 10^6 (mm^2)).

The force distribution on the upper yoke during the short-circuit condition is shown in Figure 14. The simulation results of the upper yoke deformation during a short-circuit condition is pointed out in Figure 15. It can be observed that the maximum force on the clamping beam is 9.07 N/mm.

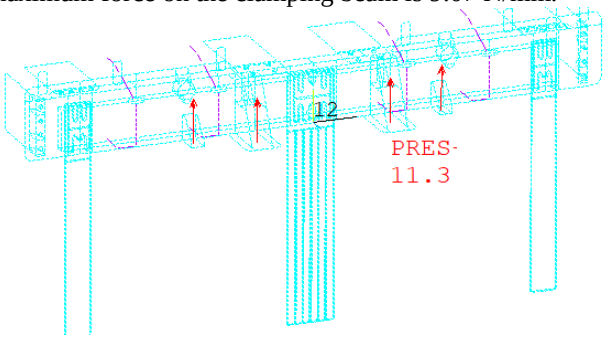

Figure 14: Force distribution on the upper yoke during the short-circuit condition.

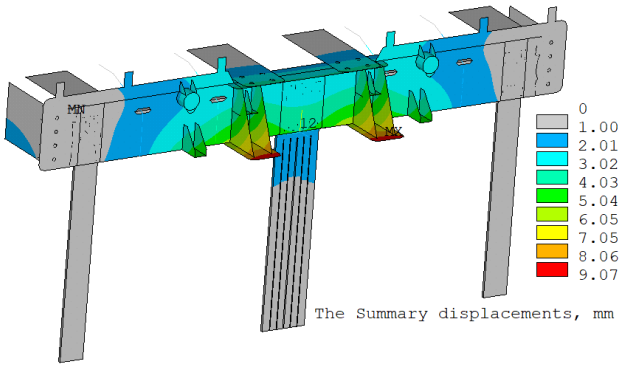

Figure 15: Simulation results of the upper yoke deformation during a short-circuit condition.

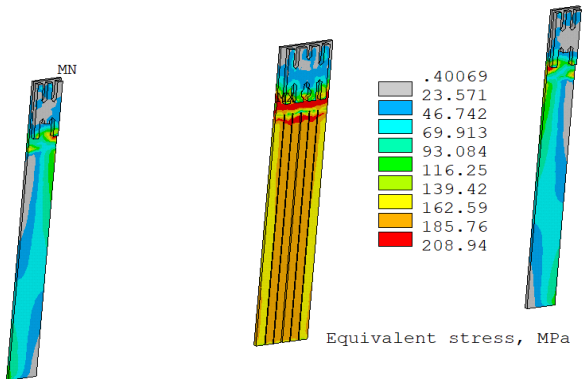

Figure 16: Results of the stresses occurring at the upper clamping plate positions during the short-circuit condition.

The results of the stresses occurring at the upper clamping plate positions during the short-circuit condition is shown in

Figure 16. In the same way, Results of the stresses occurring at the upper winding wedge positions during the short-circuit condition is presented in Figure 17. Figure 18 shows Results of the stresses occurring at the upper magnetic circuit clamping band positions during the short-circuit condition. It can be seen that the maximum stress on bandage is 437.6 Mpa.

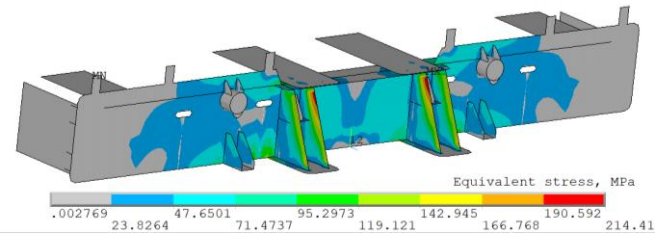

Figure 17: Results of the stresses occurring at the upper winding wedge positions during the short-circuit condition.

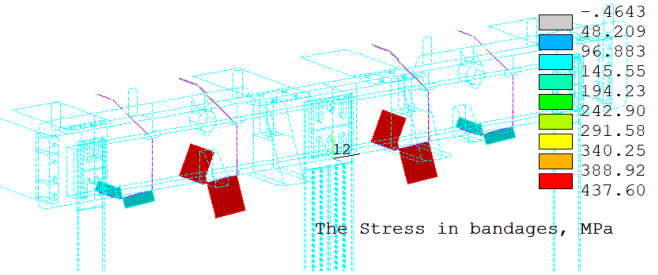

Figure 18: Results of the stresses occurring at the upper magnetic circuit clamping band positions during the short-circuit condition**.**

4.4 Simulation of lower clamping beam deformation during short-circuit conditions:

In the similar way to the upper clamping beam, the simulation of lower clamping beam deformation under the short-circuit condition is define as:

- The electrodynamic force exerted on the lower clamping beam by the low voltage (LV) winding during short-circuit conditions is: F_{LV}=309 kN.
- The electrodynamic force on lower clamping beam from the MV winding is: F_{MV}=1511 kN.
- The HV winding contributes a force on lower clamping beam is: F_{HV}=2134 kN.
- The RV winding applies a force is: F_{RV}=249 kN.
- The total short-circuit force transmitted to the lower clamping beam from all windings is therefore:

$$\sum F_{total} = F_{LV} + F_{MV} + F_{HV} + F_{RV} \quad (19)$$

=309 kN+1511 kN+2134 kN+249 kN = 4203 kN

- So, the pressure exerted on the yoke wall during a short circuit.

$$P_5 = \frac{\sum F_{total}}{4S_1} = \frac{4203000}{2x0{,}395x10^6} = 5{,}32\frac{N}{mm^2}, \quad (20)$$

where S_1 is the area of the four contact surfaces (S_1 = 0.395. 10^6 (mm^2)).

The force value and distribution on the lower yoke during the short-circuit condition is indicated in Figure 19 and Figure 20. The results of the stresses occurring at the lower clamping plate and the winding positions during the short-circuit condition are shown in Figure 21 and Figure 22. The results of the stress in bandages occurring at the lower clamping plate positions during the short-circuit condition is shown in Figure 23, with maximum value of 94,89 Mpa. The maximum values of deformation and stress in the structural components of the pressing yoke corresponding to each case are described in Table 1.

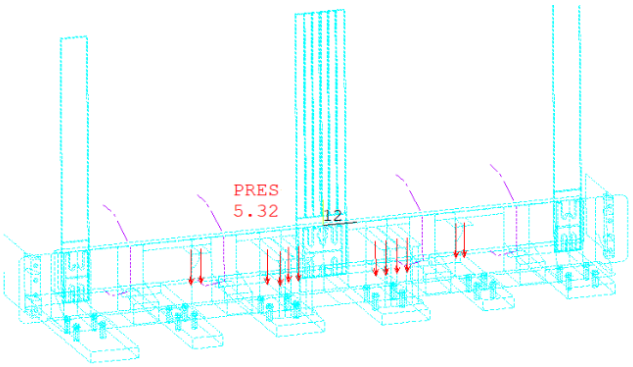

Figure 19: Force distribution on the lower yoke during the short-circuit condition.

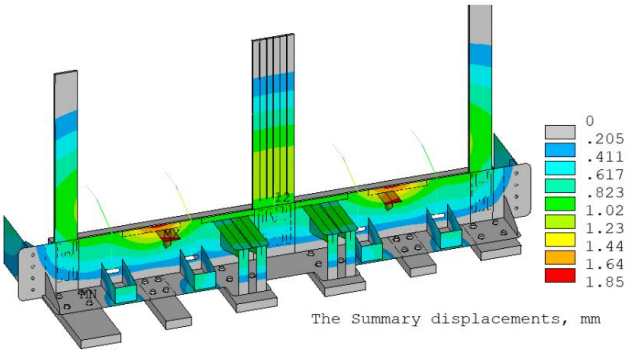

Figure 20: Simulation results of the lower yoke deformation during the short-circuit condition.

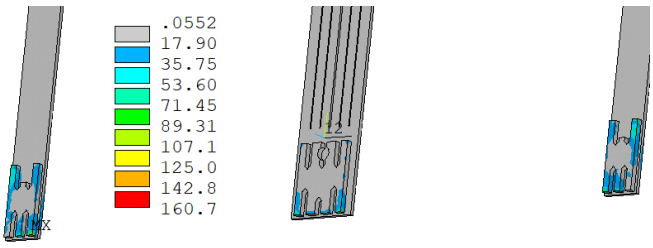

Figure 21: Results of the stresses occurring at the lower clamping plate positions during the short-circuit condition.

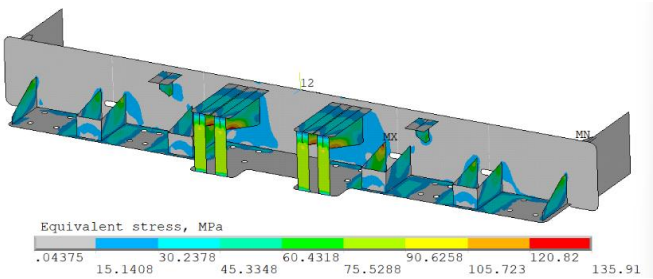

Figure 22: Results of the stresses occurring at the winding support plate positions during the short-circuit condition.

Based on the obtained results, it can be observed that with the selection of steel as the yoke material, having bending stress limits of σ_1 = 240 MPa and σ_1 = 355 MPa, and applying a safety factor of k_1 = 0.9, the allowable stress limits are determined to be 216 MPa and 319.5 MPa, respectively. The simulation results indicate that the stresses occurring in the yoke under clamping, lifting, and short-circuit conditions do not exceed these allowable bending stress limits. This

confirms that both the structural design and the selected material for the transformer yoke meet the required safety and performance standards.

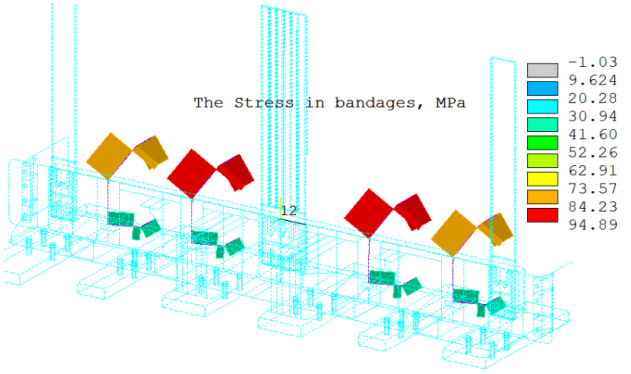

Figure 23: Results of the stresses occurring at the lower clamping band positions during the short-circuit condition.

Table 1: Results of the stresses at the lower and upper clamping beam with different positions during the short-circuit condition.

Name of clamping beam	Simulated conditions	Degree of deformation (mm)	Stress at the yoke clamping plate location (MPa)	Stress at the winding press-block (MPa)	Stress at core clamping zones (MPa)
Upper clamping beam	Winding compression	3.59	175.8	93.2	197.4
	Core and winding	2.98	176.1	66.8	171.4
	Short-circuit condition	9.07	208.9	214.4	437.6
Lower clamping beam	Short-circuit condition	1.85	160.7	135.9	94.89
Allowable stress (MPa)			0.9 x 240 = 216	0.9 x 355 = 319.5	3000

5. Conclusion

This study comprehensively analyzes the electrodynamic forces acting on the clamping beams of the power transformer rated up to 300 MVA-500kV under multiple critical operating scenarios, including winding compression, core lifting, and short-circuit conditions. By integrating analytical formulations with FEM simulations, the research accurately identifies stress concentrations and deformation patterns within the upper and lower clamping structures. The simulation results indicate that, under all evaluated conditions, the mechanical stresses remain within the allowable limits defined by the selected materials (AH36 steel and SUS304 stainless steel), with safety factors duly considered. Notably, even under extreme short-circuit forces amounting to 3,711 kN and 4,203 kN for the upper and lower clamping beams, respectively the structure maintained integrity without exceeding yield stress thresholds. These findings validate the suitability of the current design and material selection for ensuring structural reliability and operational safety. Moreover, the proposed methodology offers a reliable framework for optimizing future transformer designs and reinforces the potential of domestic manufacturing to meet the rising demand for high-capacity, supper high-voltage equipment in Vietnam's power grid modernization efforts.

Acknowledgement

The research content of this paper was supported by the results of the state-level project coded: DAĐL.CN-05/21.

References

[1] B. Doan Thanh, "Determination of winding destroy limit area for a power series of amorphous core transformers", *JMST*, vol. 103, no. 103, pp. 11–21, May 2025.

[2] T. Bao Doan and C. Phi Do, "Calculation of the Magnetic Field and Inrush Current in a Three-phase Transformer," *2020 Applying New Technology in Green Buildings (ATiGB)*, Da Nang, Vietnam, 2021, pp. 94-99.

[3] B. D. Thanh, C. P. Do, H. D. Hoan and L. T. Hiep, "Analysis of Current and Electromagnetic Force Acting on Winding in Cases of Short Circuits of Amorphous Transformer," *2023 8th International Scientific Conference on Applying New Technology in Green Buildings (ATiGB)*, Danang, Vietnam, 2023, pp. 201-208.

[4] Thanh, B. D., Le, T. H., Quoc, V. D. (2024). 'A Comparative Analysis of Axial and Radial Forces in Windings of Amorphous Core Transformers', *International Journal of Engineering*, 37(1), pp. 201-212. doi: 10.5829/ije.2024.37.01a.18.

[5] Andrei Marinescu and Carmen Livia Ungureanu, "About Axial Clamping force Mornitoring at Power Transformer Windings During Their Active LifeTime', Annals of the University of Craiova, Electrical Engineering series, No. 32, 2008, pp. 56-61.

[6] A. Marinescu, HV Power Transformer Direct Monitoring of Winding. Axial Clamping Forces, CMD 2006, Changwong, Koreea, April 2006, Paper PT 102.

[7] A. Marinescu, Monitoring of Axial Clamping Force at Power Transformer, Euro DOBLE Colloquivm, London, October 2006.

[8] Khrennikov, A & Aleksandrov, N.M.. (2019). Calculation of the electrodynamic forces causing deformation of the power transformer's windings. E3S Web of Conferences. 124. 05020. 10.1051/e3sconf/201912405020.

[9] Y. Zhai, R. Zhu, Q. Li, X. Wang, Y. Gu and S. Li, "Simulation Research on Electrodynamic Force and Deformation of Transformer Windings under Short-circuit Condition," *2022 IEEE International Conference on High Voltage Engineering and Applications (ICHVE)*, Chongqing, China, 2022, pp. 1-4

[10] Y. Zhao, T. Wen, Y. Li, H. Ni, Q. Zhang and W. Chen, "A FEM-based simulation of electromagnetic forces on transformer windings under short-circuit," *2018 IEEE International Power Modulator and High Voltage Conference (IPMHVC)*, Jackson, WY, USA, 2018, pp. 425-429

[11] Y. Li, Q. Xu and Y. Lu, "Electromagnetic Force Analysis of a Power Transformer Under the Short-Circuit Condition," in *IEEE Transactions on Applied Superconductivity*, vol. 31, no. 8, pp. 1-3, Nov. 2021, Art no. 0603803.

[12] Y. Zhao *et al.*, "Short-Circuit Electromagnetic Force Distribution Characteristics in Transformer Winding Transposition Structures," in *IEEE Transactions on Magnetics*, vol. 56, no. 12, pp. 1-8, Dec. 2020, Art no. 8400708.

[13] K. Dawood and G. Komurgoz, "Investigating effect of Electromagnetic Force on Sandwich Winding Transformer using Finite Element Analysis," *2021 28th International Workshop on Electric Drives: Improving Reliability of Electric Drives (IWED)*, Moscow, Russia, 2021, pp. 1-5.

[14] M. Jin *et al.*, "Influence of Frequency Components of Short-Circuit Electromagnetic Force on Vibration Characteristics of Power Transformer Windings," *2022 IEEE International Conference on High Voltage Engineering and Applications (ICHVE)*, Chongqing, China, 2022, pp. 01-04.

[15] M. Nazmunnahar, S. Simizu, P. R. Ohodnicki, S. Bhattacharya and M. E. McHenry, "Finite-Element Analysis Modeling of High-Frequency Single-Phase Transformers Enabled by Metal Amorphous Nanocomposites and Calculation of Leakage Inductance for Different Winding Topologies," *in IEEE Transactions on Magnetics*, vol. 55, no. 7, pp. 1-11, July 2019, Art no. 8401511.